Nanoscale

Accepted Manuscript

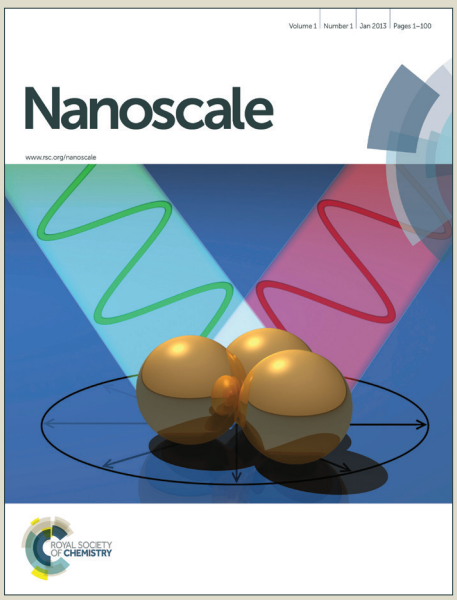

ROYAL SOCIETY OF CHEMISTRY

www.rsc.org/nanoscale

One-Pot Synthesis of High-Index Faceted AgCl Nanocrystals with Trapezohedral, Concave Hexoctahedral Structures and Their Photocatalytic Activity

Haibin Zhang,* Yonggang Lu, Hong Liu and Jingzhong Fang

Lightweight Optics and Advanced Materials Center, Institute of Optics and Electronics, Chinese Academy of Sciences, Chengdu, 610209, People's Republic of China.

* Address correspondence to E-mail: zhb@ioe.ac.cn

AgCl semiconductor nanocrystals (NCs) with trapezohedral (TPH) and concave hexoctahedral (HOH) structures have been successfully synthesized for the first time in high yield by a direct one-pot solvothermal method. The as-prepared TPH, concave HOH AgCl NCs with unconventional polyhedral shapes and smooth surfaces were enclosed by 24 high-index {311} facets and 48 high-index {15 5 2} facets, respectively. The specific ionic liquids poly(diallyldimethylammonium) chloride (PDDA) acted as both Cl^- ions precursor and a morphology-controlled stabilizer, which was indispensable for the formation of these high-index faceted AgCl polyhedra and the derived uniform octahedral AgCl in the appropriate concentration of hot $AgNO_3$ ethylene glycol (EG) solution. With high-index facetes exposed, both TPH and concave HOH AgCl NCs exhibit much higher photocatalytic activity than octahedral AgCl NCs whose faces mainly exposed {111} with lower surface areas and surface energies in degradation of organics under sunlight. It is expected that the polyhedral AgCl NCs with high-index facets is an effective approach for the design alternative semiconductor photocatalysts with high performance, which may find potential applications such as in photochromics and environmental managements.

1. Introduction

Development of functional nanomaterials for solving the global energy shortage and environmental problems has become the subject of intensive research for scientists in recent years.[1-6] As one promising green technology, semiconductor photocatalysis attracts great interest in many photocatalytic applications, such as clean energy regeneration,[7] water disinfection,[8] and organic containments purification.[9] Generally, most semiconductor photocatalytic work are focused on the transient metal oxide

semiconductors with large band gaps and high-energy ultraviolet (UV) light is required to ensure the photocatalytic activity of photocatalysts, limiting their effective applications driven by solar energy concentrated in visible light regions. Although modified strategies, i.e., controlled morphology,[10] elemental doping[11] and surface sensitization[12] have been devoted to improve the absorption coefficient of photocatalysts in visible light, the complicated synthetic processes with limited enhancement lose their charm in the large-scale practical applications. As a result, one promising way is to design an alternative photocatalysts with facile synthesis and good efficiency.

Since Huang and coworkers[13] reported Ag@AgCl particles as an active plasmonic photocatalyst, silver halides (AgX, X = Cl, Br, I) have been found to be one of the most promising photocatalytic alternatives to traditional semiconductor photocatalysts. To date, AgCl NCs with various morphologies,[14-16] ternary alloyed $AgCl_xBr_{1-x}$ NCs,[17] AgI/Ag_3PO_4 heterocrystals,[18] etc. have been successfully synthesized and their photocatalytic activity in degradation of organic containments under visible light irradiation were exhibit remarkably. However, to the controllable synthesis of complicated structures with high surface areas and surface energies, and the corresponding photocatalysis studies, until now, there have been few reports on high-index faceted polyhedral silver halide nanocrystals, especially for AgCl NCs. As is known, nanocrystals enclosed with high-index facets usually hold a high catalytic activity thanks to the high density of low-coordinated step atoms that they exposed on their surfaces.[19-20] Meanwhile, high-index facets normally grow faster during a crystal growth stage and thus are preferentially eliminated to minimize total surface energies of the final NCs.[21] Therefore it presents a big challenge to synthesize high-index faceted polyhedral AgCl NCs with a controlled morphology and investigate their resultant behaviors.

Herein, we report, for the first time, a facile one-pot approach for the high-yield fabrication of AgCl NCs with perfect high-index faceted TPH and concave HOH structures, which enclosed by 24 high-index {311} facets and 48 high-index {15 5 2} facets, respectively. As far as we know, such unconventional polyhedral constructions were only appeared in the studies about noble metal nanocrystals,[21-25] which have not been reported in semiconductor photocatalysts. Depending on the specific ionic liquid surfactant PDDA and the appropriate concentration of $AgNO_3$ precursor in hot EG solutions, high-index faceted AgCl NCs were formed, and the derived products such as octahedral AgCl NCs enclosed by {111} facets, disordered AgCl or Ag based nanorods and nanoparticles (NPs) can be produced as well. Through the photocatalytic tests, it can be found that both TPH and concave HOH AgCl NCs exhibit much higher photocatalytic activity than that with octahedral morphologies in degradation of organic dye methyl orange (MO) under sunlight owing to the existence of high index facets with higher surface areas and surface energies.

2. Experimental section

2.1 Chemicals

Silver nitrate ($AgNO_3$, 99.99%), Methyl Orange (MO) was obtained from Aladdin Chemical Regent Co. Ltd (Shanghai,China). Anhydrous ethylene glycol (EG, ⩾99%), Poly(diallyldimethylammonium) chloride (PDDA, MW=400000–500000 D, 20 wt% in H_2O, ⩾99%) were purchased from Sigma-Aldrich. All regents were analytical grade and used as received without further purification. The deionized water with a resistivity of 18 MΩ cm was used in all experiments.

2.2 Synthesis of TPH, concave HOH AgCl NCs and their derivatives

The AgCl samples were prepared based on a ionic liquid surfactant PDDA[26,27] assisted polyol system. In a primary reaction, 0.8 mL portion of PDDA was added to 20 mL of EG solution in a brown glass flask. The mixture was stirred with a magnetic blender for 1–2 min at room temperature and ambient conditions. Next, a 1 mL aliquot of $AgNO_3$ solution in EG was introduced under stirring. The resulting mixture was sealed and subsequently refluxed at 200 ℃ for 2h. The final solution was cooled, and the white products were collected by centrifugation (12000 rpm, 15 min) and washed repeatedly with water. Then the final samples were resuspended in water or ethanol for further characterizations.

Different concentrations of $AgNO_3$ solution in EG were used for the synthesis of TPH (100 mM, $AgNO_3$/PDDA molar ratio = 1/10), octahedral (50 mM, $AgNO_3$/PDDA molar ratio = 1/20), concave HOH (20 mM, $AgNO_3$/PDDA molar ratio = 1/50) AgCl NCs and disordered AgCl or Ag based (5 M, $AgNO_3$/PDDA = 5/1 ; 10 M, $AgNO_3$/PDDA = 10/1) derivatives.

2.3 Evaluation of photocatalytic performance

The photocatalytic performance of AgCl NCs was evaluated through degradation of organic dye MO using a 300W Xe arc lamp equipped with a UV cut-off filter as the source of visible light (λ⩾400 nm). In a typical procedure, 10 mg of the AgCl sample was dispersed in 50 mL of MO aqueous solution (20 mg L^{-1}) by sonication. Before the degradation reaction was carried out, the suspension was kept stirring in the dark until the dye absorption equilibrium on the surface of the catalysts was reached. The mixture was then exposed to visible light and aliquots of the solution (2 mL) at given time-intervals were taken out. Each sampling solution centrifuged at 12000 rpm for 15 min to settle the nanoparticles at the bottom of the centrifuge tube and the top solution was transferred to a quartz cuvette for UV-Vis absorption measurement.

2.4 Characterization

The structures and morphologies of as-prepared samples were performed on X-ray diffraction (XRD, Bruker D8/DISCOVER X-ray diffractometer equipped with Cu-Ka radiation λ=1.5418 Å) and field emission scanning electron microscopy (FESEM, Hitachi SU8010 microscope, operated at an acceleration voltage of 5.0 kV). UV–Vis diffuse reflectance spectra light absorbance curves were recorded on a Lambda-1050

spectrophotometer in the wavelength range of 200-1000 nm. Specially, to minimize any reduction of AgCl into Ag during SEM imaging, the samples were coated with a thin platinum (Pt) layer (15 ~ 20 nm) and the imaged only for a short period of time (~ 10 sec).

3. Results and discussion

3.1 Structural characterization

Polyhedral AgCl NCs enclosed by two classes of high-index facets could be formed in high yield by adjusting the $AgNO_3$/PDDA molar ratio, i.e., the concentration of $AgNO_3$ in EG solution.

Fig. 1 presents the typical SEM images of as-prepared TPH AgCl NCs and a histogram of particle size distribution when $AgNO_3$/PDDA=1/10. It can be seen that the yield of AgCl NCs with TPH shape is nearly 100%, and TPH AgCl NCs show a narrow size distribution with an average particle size of 1.05 μm (Fig. 1g). The three-dimensional structure of TPH AgCl NCs with smooth surfaces is clearly visible in the high-magnification SEM image (Fig. 1b). The good agreement between the SEM images of the different oriented NCs and the geometrical models (shown on the right of each image) confirms the TPH geometry of AgCl NCs (Figure. 1c-e). In fact, previous research about high-index faceted noble metal nanocrystals has shown that TPH structure is an unconventional polyhedron bounded by 24 high-index {hkk} (h>k) facets.[21,22] To identify the specific Miller indices of TPH NCs, in theory, the straightforward approach is via the characterization of TEM and the corresponding selected-area electron diffraction (SAED). However, this can not be realized to our particular AgCl NCs because exposing the AgCl to an electron beam with high current density (for zoom-in observation) for a long time always reduces AgCl to metallic Ag.[16] Therefore, another facile and effective approach was considered, which was to measure the angles of projections along an appropriate crystallographic axis.[25] For the TPH AgCl NCs, the optimal projective direction is along <100>, resulting in an octagon with 4-fold symmetry. The projection angles of TPH AgCl NCs along <100> direction (Fig. 1f) can be used to determine the corresponding Miller indices. Through the accurate measurement, the average values of α and β are 143.3° and 126.8°, respectively, which agrees well with the corresponding theoretical values of {311} facets. These above results imply that the synthesized AgCl NCs have a TPH structure with 24 high-index {311} facets. Probably it may be questioned that whether the TPH NCs are metallic Ag according to the synthesized experience in a polyol system assisted by surfactants.[29] Clearly, the XRD patterns (shown in Fig. 3c) which exhibit sharp diffraction peaks corresponding to the {111}, {200}, {220}, {311}, {222}, {400}, {331} and {420} planes (JCPDS file: 31-1238), indicating that the TPH NCs are pure face-centered cubic (fcc) AgCl crystals rather than Ag crystals. That is, AgCl NCs existed stably and has not been reduced to metallic Ag in this preparation.

When the $AgNO_3$/PDDA molar ratio was reduced to 1/50, the shape of the AgCl NCs transformed from TPH to concave HOH structure, which can be seen in the SEM

images of Figure. 2. The yield of the concave HOH AgCl NCs is also very high (more than 98%) and the size (~1.15 μm) is similar to TPH AgCl NCs with a narrow size distribution (Fig. 2g). It is well known that a conventional HOH structure can be considered as a trisoctahedra (TOH) with its <111> edges bending outward from the edge centers.[23] Particularly, a new class of concave HOH structures, which can be visualized as a octahedra with its {111} facets bending inward from the facet centers, shown in our synthesis (Fig. 2b). The concave HOH geometry was also confirmed by the good agreement between the SEM images of the AgCl NCs and the geometrical models of concave HOH shape in the same orientation (Figure. 2c-e). Furthermore, the projection angles of concave HOH AgCl NCs viewed from the <110> direction (Fig. 2f) are used to describe the HOH Miller indices {hkl} (h>k>l). Measurement reveals that the average values of α, β and γ are 194.1°, 74.9° and 163.95°, respectively, which agrees well with the theoretical values of {15 5 2} facets. Confirmed by the XRD patterns shown in Fig. 3a, the as-prepared concave HOH NCs also exhibit a pure fcc AgCl structure. Thus, it can be indicated that the unique concave polyhedron NCs are concave HOH structure AgCl NCs with 48 high-index {15 5 2} facets.

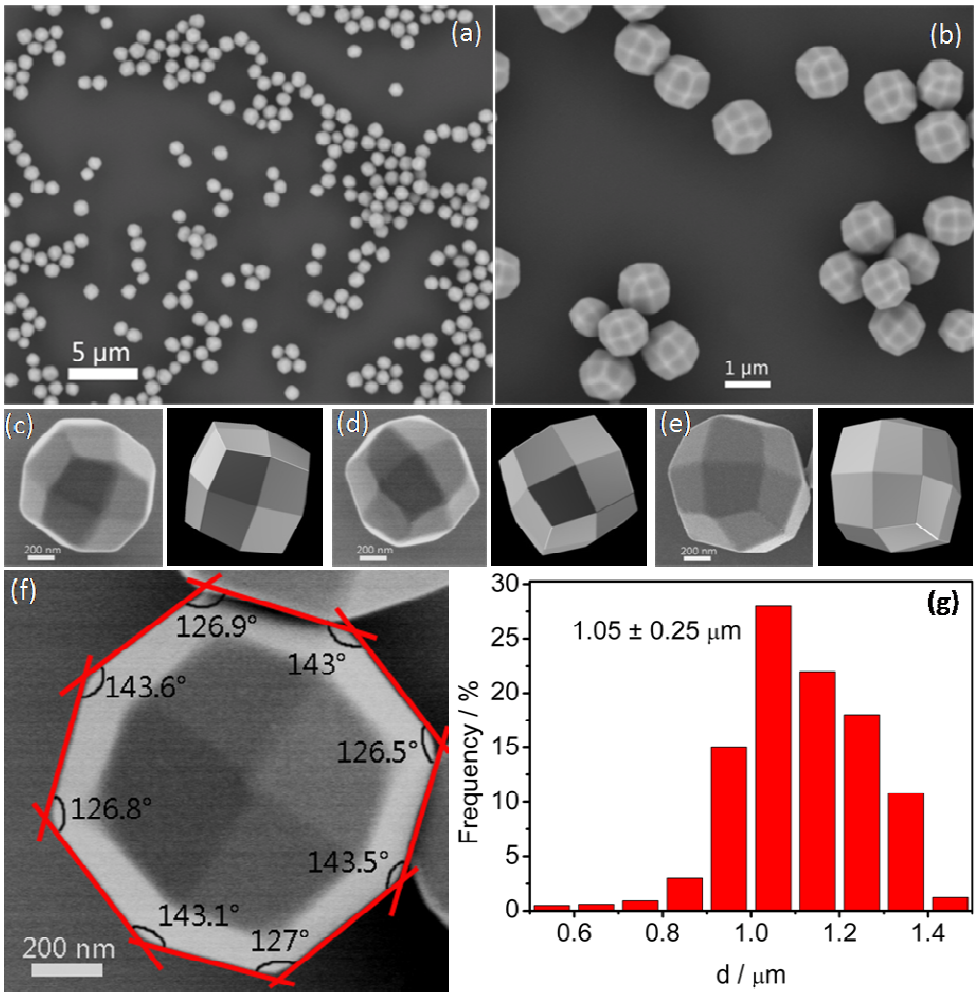

Fig.1 (a-b) Typical SEM images of TPH AgCl NCs: (a) large-area, (b) enlarged. (c-e)

Individual NCs in different orientations, with the corresponding geometrical models shown on the right of each SEM image. The scale bar is 200 nm. (f) A single TPH AgCl NCs viewed from the <100> direction. (g) Size distribution of the as-prepared TPH AgCl NCs.

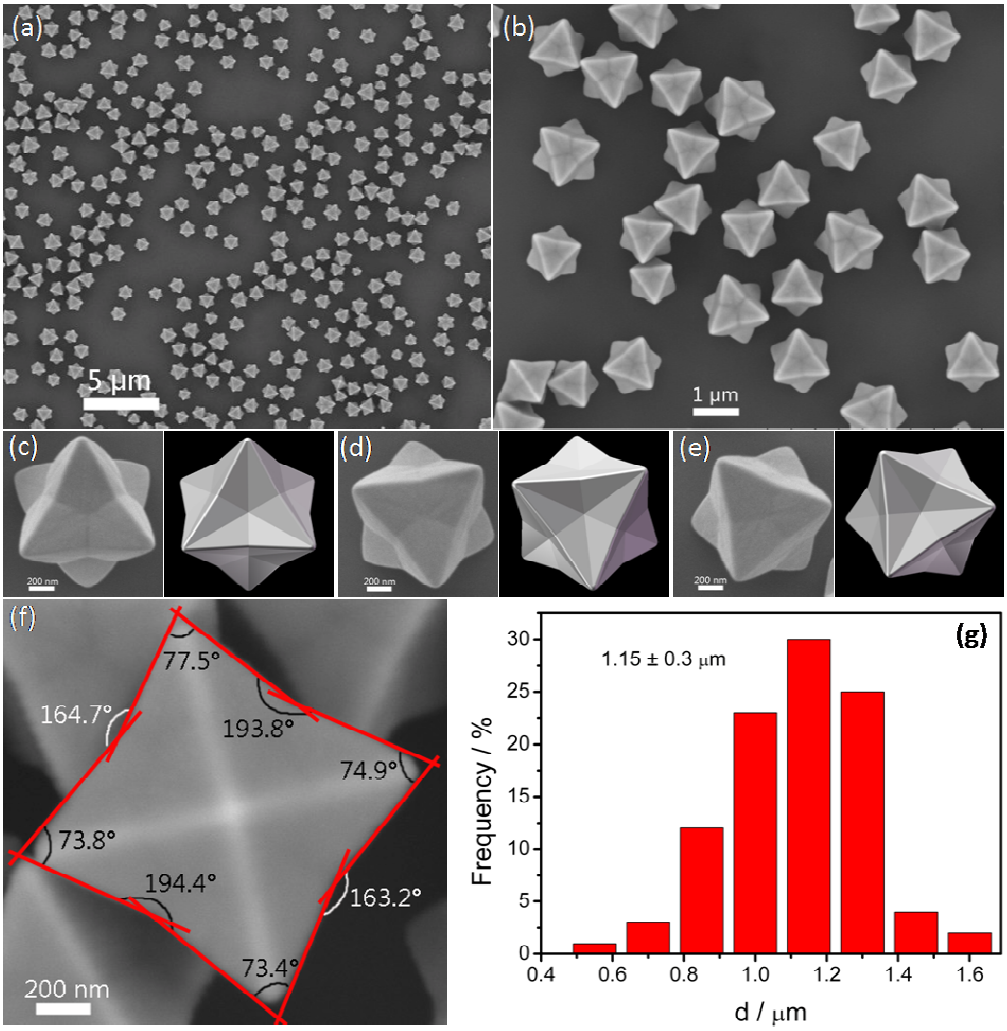

Fig. 2 (a-b) Typical SEM images of concave HOH AgCl NCs: (a) large-area, (b) enlarged. (c-e) Individual NCs in different orientations, with the corresponding geometrical models shown on the right of each SEM image. The scale bar is 200 nm. (f) A single concave HOH AgCl NCs viewed from the <110> direction. (g) Size distribution of the as-prepared concave HOH AgCl NCs.

In addition, various derivatives including octahedra, nanorods and irregular NPs can be produced during the preparation of high-index faceted AgCl NCs (as shown in Fig. 4). The overview SEM image (Fig. 4a) of AgCl NCs presents the high yield of uniform octahedral structure, with the size of ~1 μm, when adjusted the molar ratio

$AgNO_3$/PDDA=1/20. The enlarged image (Fig. 4b) reveal clearly that each octahedral surface is smooth and has a slightly concavity. Typical XRD patterns (Fig. 3b) shows that the octahedral NCs maintained AgCl structure. Two strongest Bragg diffraction peaks from {111} and {222} planes suggests that the octahedral AgCl NCs preferred orientation growth along <111> direction, which has been similarly demonstrated in the past noble NCs research.[27] Hence, we believe that the uniform AgCl octahedra with a slightly concavity is an intermediate between TPH and concave HOH AgCl. Specially, as the molar ratio of $AgNO_3$ and PDDA increased, where there was excess amount of Ag^+ ions compared to Cl^- ions, undesirable results were obtained. Fig. 4c displays the typical SEM image of the products under high concentration of $AgNO_3$ conditions ($AgNO_3$/PDDA=5/1). It can be seen that the as-synthesized NCs losed their regular polyhedral morphologies, and the disordered NPs with wide size distribution appeared. The corresponding XRD patterns (as illustrated in Fig. 3d) demonstrates that these disordered NPs are comprised of two types of crystals, that is, fcc AgCl and fcc Ag. Meanwhile, we can find that the relative intensity of Ag diffraction peaks is higher than AgCl, indicating that the main components of as-prepared disordered products are Ag NPs, and of course contain a little AgCl NCs. Further increasing the $AgNO_3$/PDDA molar ratio to 10/1, vast crystalline Ag NPs and a much smaller amount of AgCl NCs with rod-like and irregular shapes were presented, which can be seen from Fig. 3e and Fig. 4d.

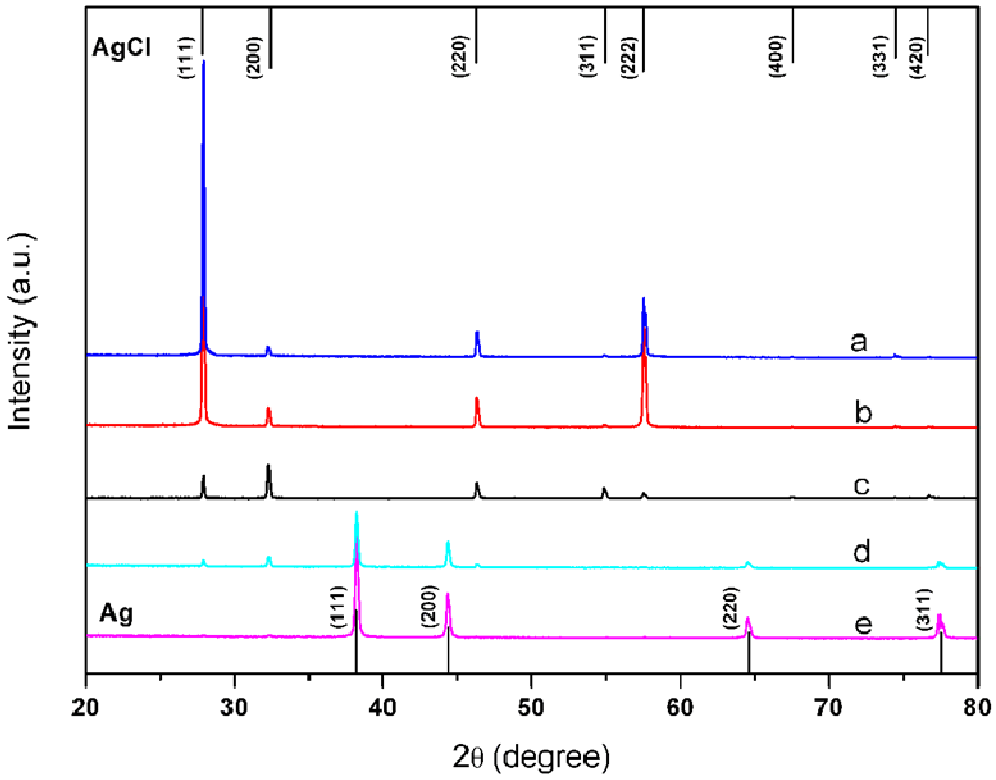

Fig. 3 XRD patterns of high-index faceted AgCl and AgCl or Ag based derivatives obtained with different molar ratio of $AgNO_3$ and PDDA: (a) 1:50, (b) 1:20, (c) 1:10,

(d) 5:1 and (e) 10:1. The top and bottom marked lines are standard AgCl (JCPDS file: 31-1238) and Ag (JCPDS file: 04-0783) patterns.

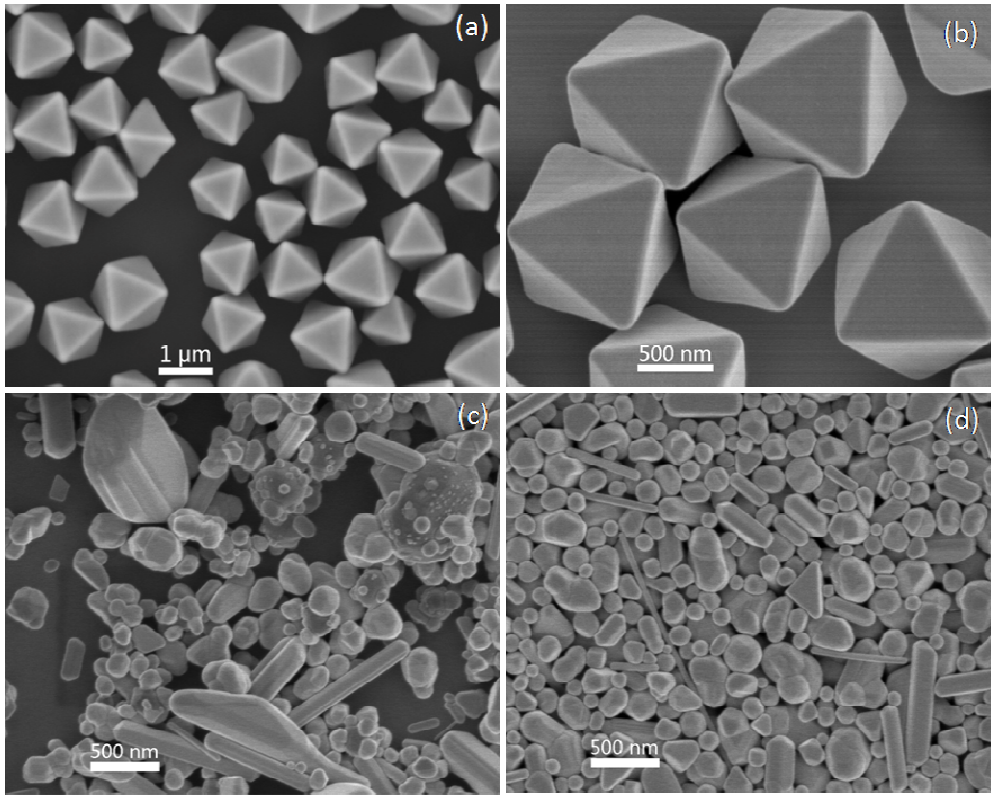

Fig. 4 SEM images of prepared octahedral AgCl NCs in (a) low and (b) high magnifications. Typical SEM images of AgCl and Ag based products synthesized with different molar ratio of $AgNO_3$ and PDDA: (c) 5:1 and (d) 10:1.

3.2 Effects of reaction temperatures and times

To detailed discuss the specific formation of TPH and concave HOH AgCl NCs, experiments under different reaction temperatures and times were thus conducted in this study. As shown in Fig. 5 and 6, a series of AgCl products were presented when we kept the same TPH or concave HOH AgCl NCs formation molar ratio $AgNO_3$/PDDA under different reaction temperatures. AgCl NPs with size of 100~200 nm were formed in the synthesis of high-index faceted TPH and concave HOH AgCl without heating process, the reaction temperature was room temperature, 25 ℃ (Fig. 5a and 6a). When the temperature was low, T=90 ℃, near-spherical AgCl NPs with wide size distribution (60~300 nm) were obtained in Fig. 5b, 300~600 nm of near-spherical and octahedral AgCl NPs were mixed in Fig. 6b. When further adjusting of reaction temperature to 160 ℃, the main products were 600~800 nm of polyhedral AgCl and a small amount of typical TPH construction with size of ~ 1 μm were appeared in Fig. 5c. Besides, ~ 1 μm of octahedral AgCl were high-yield formed

again in Fig. 6C. If slightly reduced the reaction temperature to 180 ℃, the sizes of AgCl products were still uniform (~ 1μm), while, the shapes were few TPH and mainly tended to polyhedral growth as shown in Fig. 5d. On the other hand, concave HOH morphologies were not obvious, even existing of octahedral construction in Fig. 6d. Above all, it can be deduced that low reaction temperature leaded to the slow nucleation and crystal growth of AgCl nucleis, which tended to the high-yield fabrication of AgCl NPs, yet higher temperature increased the reaction power of polyol system so that AgCl nucleis could be formed and aggregated rapidly, then the relatively higher diffusion constant and the role of surplus PDDA would provide a possibility for the specific growth of these nucleis to form the desired high-index faceted AgCl NCs.

Furthermore, typical TPH AgCl NCs formed under different reaction times from 0 min to 5h were collected to further understand the nucleation and crystal growth process as shown in Fig. 7. We found that near-spherical nanoparticles with size of ~ 200 nm were formed before the reaction mixture was refluxed at 200 ℃ (Fig. 7a), which was in agreement with the room temperature results. When the reflux at 200 ℃ for 5 min, the sizes (~ 600 nm) were increased and the initial polyhedral shapes appeared (Fig. 7b). Further growth and aggregation made these initial polyhedron into regular TPH morphologies with size of ~ 800 nm in 30min (Fig. 7c). Panels (d) and (e) from Fig. 7 shows the nanostructures obtained at 2 and 5 h, respectively. Clearly, ~ 1 μm of typical TPH AgCl NCs with uniform sizes and perfect shapes were formed after 2h passed. Typical TPH structures were stabilized when the reaction was maintained for 5h. It means that the whole nucleation and growth of typical TPH AgCl NCs lasted for about 2h.

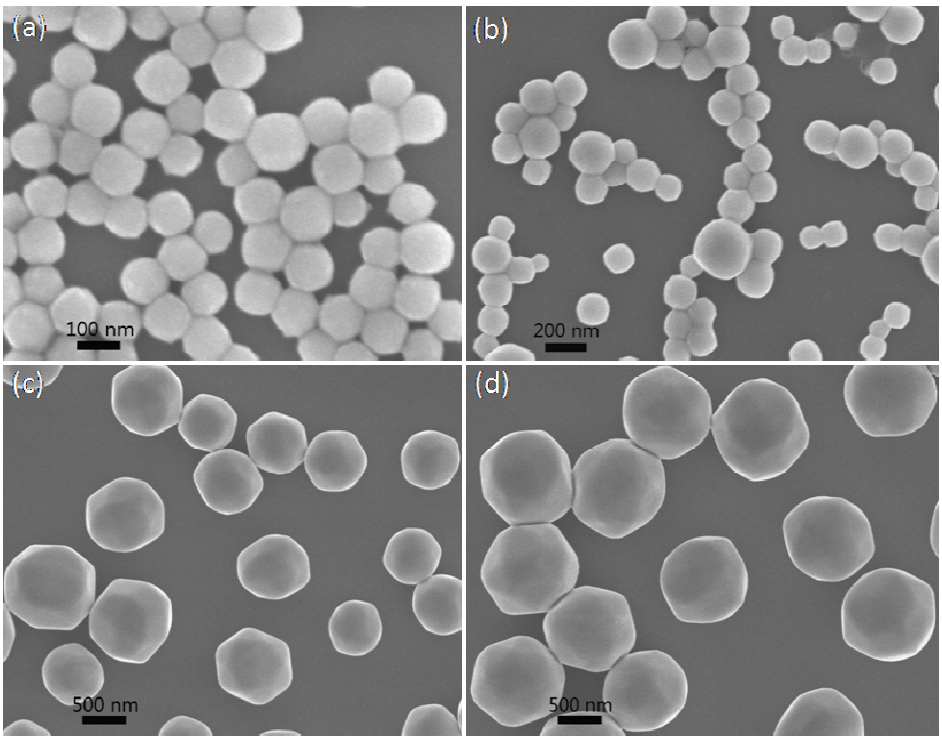

Fig. 5 SEM images of prepared products synthesized in the same TPH AgCl NCs formation molar ratio $AgNO_3$/PDDA=1/10 under different reaction temperatures: (a) T=25 ℃, (b) T=90 ℃, (c) T= 160 ℃ and (d) T=180 ℃.

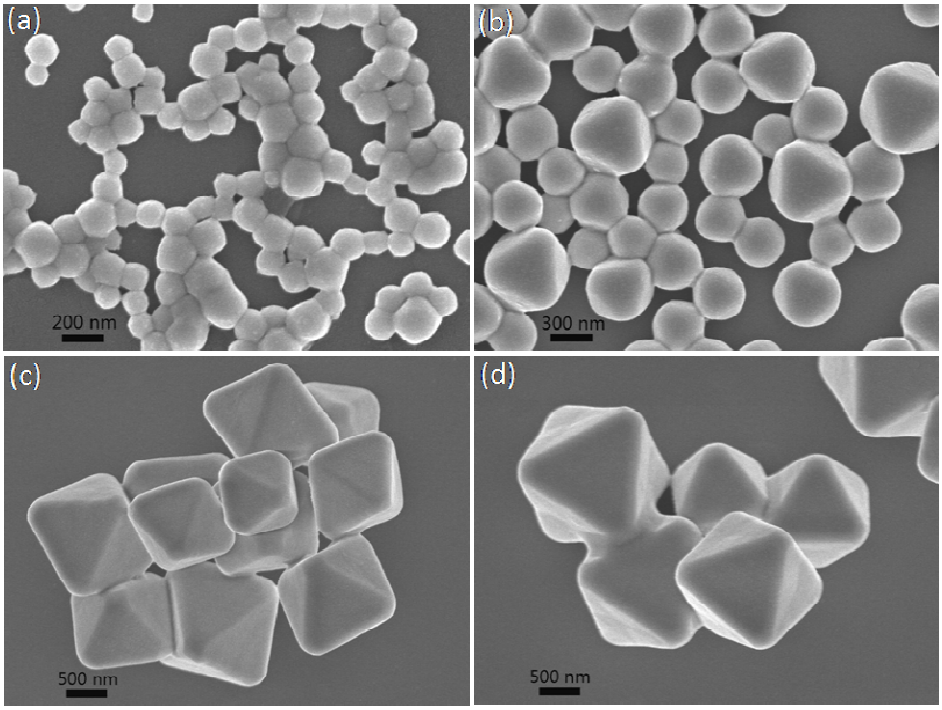

Fig. 6 SEM images of prepared products synthesized in the same concave HOH AgCl NCs formation molar ratio $AgNO_3$/PDDA=1/50 under different reaction temperatures: (a) T=25 ℃, (b) T=90 ℃, (c) T= 160 ℃ and (d) T=180 ℃.

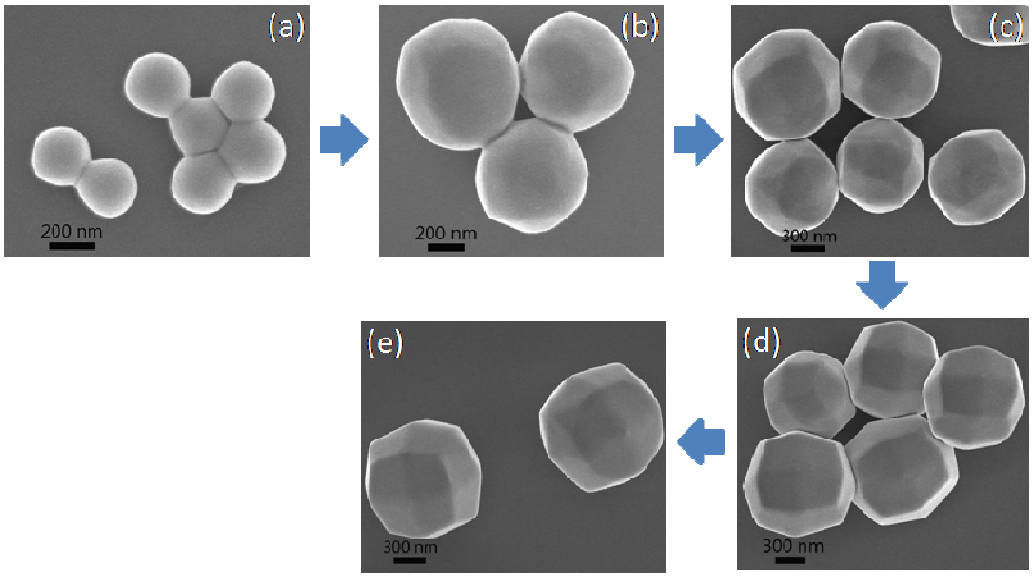

Fig. 7 SEM images for the shape evolution of typical TPH AgCl NCs at different reaction times: (a) t=0 min, (b) t=5 min, (c) t= 30 min, (d) t= 2 h and (e) t= 5 h.

3.3 Formation mechanism

On the basis of the above results, we proposed a possible formation mechanism of high-index faceted AgCl NCs and their derivatives as follows. Firstly, excessive PDDA molecules relative to $AgNO_3$ in the polyol system is indispensable for the formation of TPH, concave HOH and octahedral AgCl NCs. In our synthesis, PDDA was introduced to the reaction as both Cl^- sources and stabilizer, which would play an important role as a strong shapecontroller to assist the crystal growth.[28] Once $AgNO_3$ mixed with abundant PDDA, Ag^+ ions would combine with Cl^- ions (from PDDA) and the initial AgCl nucleis were formed, which were controlled through the selective adsorption of PDDA on the specic AgCl surfaces. Actually these nucleis tended to persistent growth and aggregation to form the particular AgCl NPs before the refluxing process began. Later, the high temperature refluxing conditions caused a higher diffusion constant and the surplus PDDA molecules may provide a delicate balance between nucleation ratio and diffusion ratio for the nonequilibrium, favoring the kinetically controlled process of high-index faceted AgCl polyhedral and octahedral growth. Specially, PDDA molecules preferentially absorbed on the specific planes of AgCl nucleis, thus, the <311>, <15 5 2>, <111> direction crystal growth rate were inhibited to TPH, concave HOH and octahedral AgCl NCs, respectively (as shown in Fig. 8). On the other hand, excessive $AgNO_3$ in our reaction system tends to the formation of disordered hybrid Ag and AgCl NCs. The explanation of Ag NPs in this work is similar to the general noble metal nanocrystals preparation, which is attributed to hot reduction by polyol with the assistance of surfactants. While to the disordered and irregular morphologies, we proposed that it may be caused by the inhomogeneous fast Ag crystal growth assisted by insufficient PDDA stabilizer under high temperature. Additionally, the formation of disordered AgCl NCs may also can be considered as the initial formed small amount of AgCl nucleis tended to disordered crystal growth without excessive PDDA. Although, Sun and coworkers[16] reported a phenomenon that the partial AgCl would transform to elemental Ag through reduction with hot EG, it is worth noting that their preparation of AgCl:Ag NCs was so different, which used $AgNO_3$, NaCl as precursors and Poly(vinyl pyrrolidone) (PVP) as a stabilizer. In fact, Ag NCs produced during their synthesis was also under the condition that excess amount of Ag^+ ions compared to Cl^- ions, thus Ag^+ may be reduced by EG with the assistance of PVP, no AgCl NCs reduced to Ag NPs in hot EG solution, which has been clearly shown in our chemical composition analysis (Fig. 3a-c).

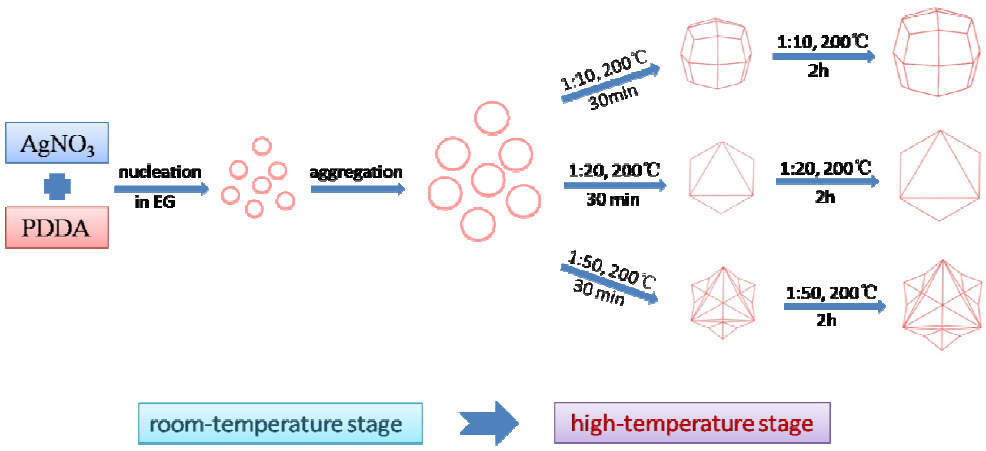

Fig. 8 The formation mechanism of TPH, octahedral and concave HOH AgCl NCs.

3.4 UV-Visible absorption spectroscopic characterization

The UV-Vis diffuse reflectance spectra light absorbance curves of TPH, concave HOH and octahedral AgCl NCs were recorded to estimate their corresponding optical properties (Fig. 9). Clearly, we can see that whether high-index faceted TPH, concave HOH or octahedral AgCl samples exhibit strong absorption in the UV light range (200-400 nm). Specially, TPH and concave HOH AgCl exhibit two strong absorption at (237 nm, 335 nm), (245 nm, 373 nm), respectively. The absorption peaks of concave HOH AgCl was red-shifted relative to TPH AgCl, suggesting that the size of concave HOH AgCl NCs increased, which has been demonstrated in Fig.2. However, the octahedral AgCl exhibits only one strong absorption at 225 nm, another absorption at 370 nm is weak. It is well known that AgCl has direct and indirect band gap of 5.15 eV (~ 240 nm) and 3.25 eV (~ 380 nm), respectively.[30] Our results agrees well with this theory values. Apparently, another weak absorption appearing in the visible range (~550 nm) to each AgCl samples. We think that the weak absorption can be attributed to the small amount of Ag NPs formed on the AgCl NCs surfaces under weak irradiation from environments during the sample preparation or measurement.

Based on the above UV-Vis absorption results, we speculate that the high-index faceted AgCl NCs may exhibit more significant performance than octahedral AgCl NCs in the future optical applications.

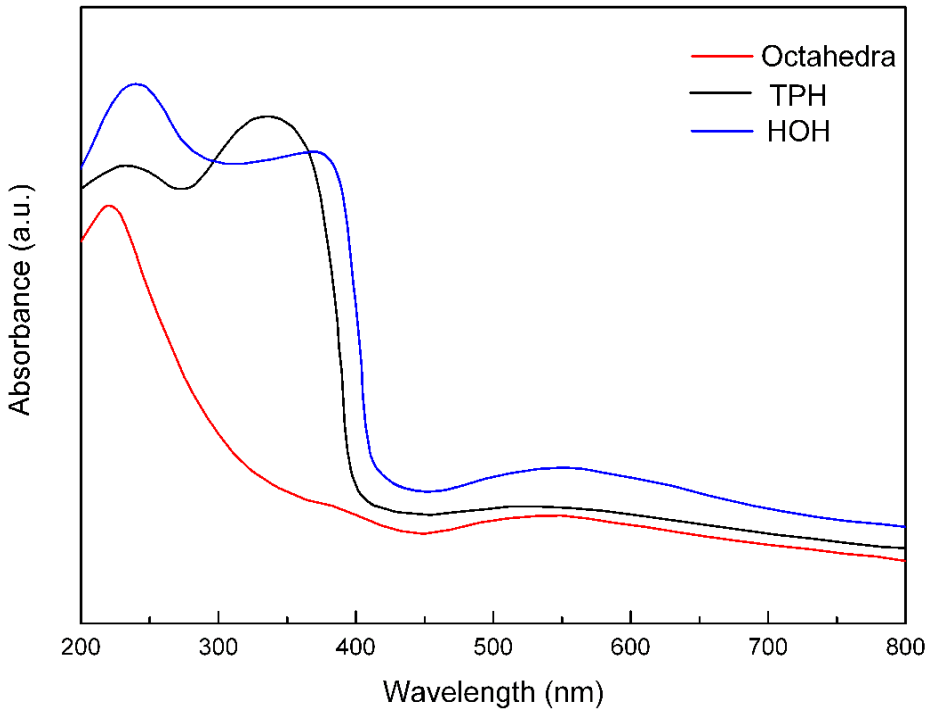

Fig. 9 UV-Visible absorption spectra of TPH (black line), concave HOH (blue line) and octahedral (red line) AgCl NCs.

3.5 Photocatalytic tests

To evaluate the photocatalytic activity of the as-prepared AgCl samples, organic dye MO was used as target substance to test their photodegradation performance under visible light irradiation ($\lambda \geqslant 400$ nm). Fig. 10A shows a series of absorption spectra of MO solution changes with various reaction times since the photocatalytic reaction started under continuous irradiation of visible light in the presence of TPH AgCl NCs. Clearly, one can find that the MO molecules can be effectively decomposed with the assistance of TPH AgCl NCs photocatalysts. When the photodegradation reaction proceeds for 80 min, the MO molecules are completely decomposed. For comparison, MO phtodegradations were also performed with octahedral AgCl NCs, concave HOH AgCl NCs and natural condition under an identical visible light exposure (Fig. 10B). The results (Fig. 10B (a-c)) indicates that the photocatalytic efficiency of MO is relatively low with the assistance of octahedral AgCl NCs photocatalysts, where 120 min is required to completely degrade MO dye. While the concave HOH AgCl NCs displayed enhanced performance compared to the same quantity of TPH AgCl NCs, where the former can decompose more than 99% MO molecules in 60 min, and the catalytic activity of concave HOH AgCl is nearly two times higher than octahedral AgCl. Furthermore, Fig. 10B (d) shows that nearly no MO can be degraded under visible light illumination without a catalyst, meaning that the dye is indeed

decomposed with the assistance of the AgCl phtocatalysts. Surely, the whole AgCl NCs assisted degradations are due to the photocatalysis, not to the directly absorption of MO on AgCl NCs, which has been demonstrated in the results of dark test. The stability of our AgCl photocatalysis were measured in ten times recycling degradation experiments, and the efficiency change is shown in Fig. 11. The three classes of photocatalysts are stable, and as the recycling times increase, the photocatalytic efficiency decreased slightly due to the slight loss of AgCl samples in every recycling experiment.[14] In a word, the AgCl NCs obtained in our preparation is active and stable as visible light-driven photocatalysts, notably, high-index faceted TPH, concave HOH AgCl NCs exhibit much higher photocatalytic activity than octahedral AgCl NCs.

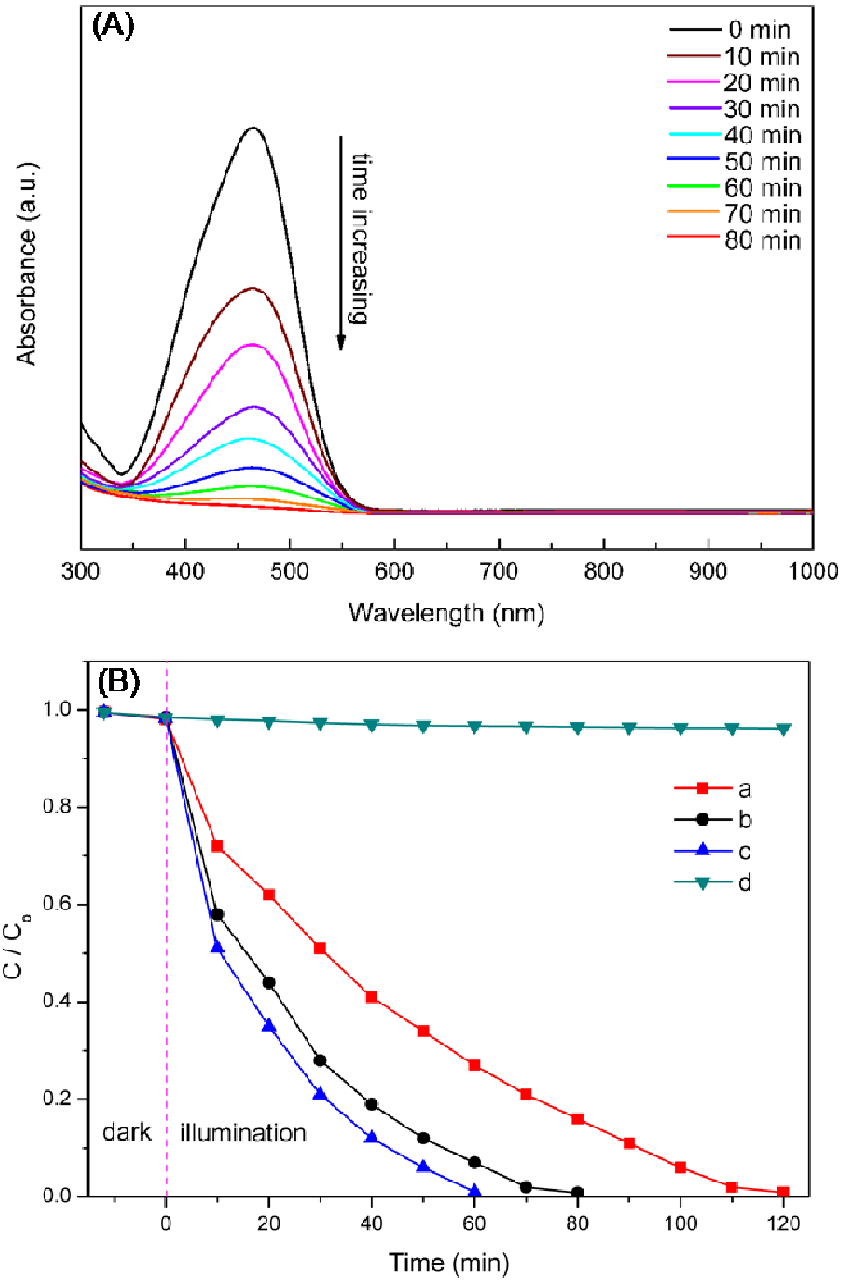

Fig. 10 (A) Absorption spectra of the MO molecules at different times since the photocatalytic reaction started under continuous illumination of visible light with assistance of the TPH AgCl NCs. (B) The comparison of MO dye photodegradation dynamics under different conditions, (a-c) under visible light irradiation with different AgCl photocatalysts: (a) octahedral AgCl NCs, (b) TPH AgCl NCs and (c) concave HOH AgCl NCs, (d) under visible light illumination without a catalyst.

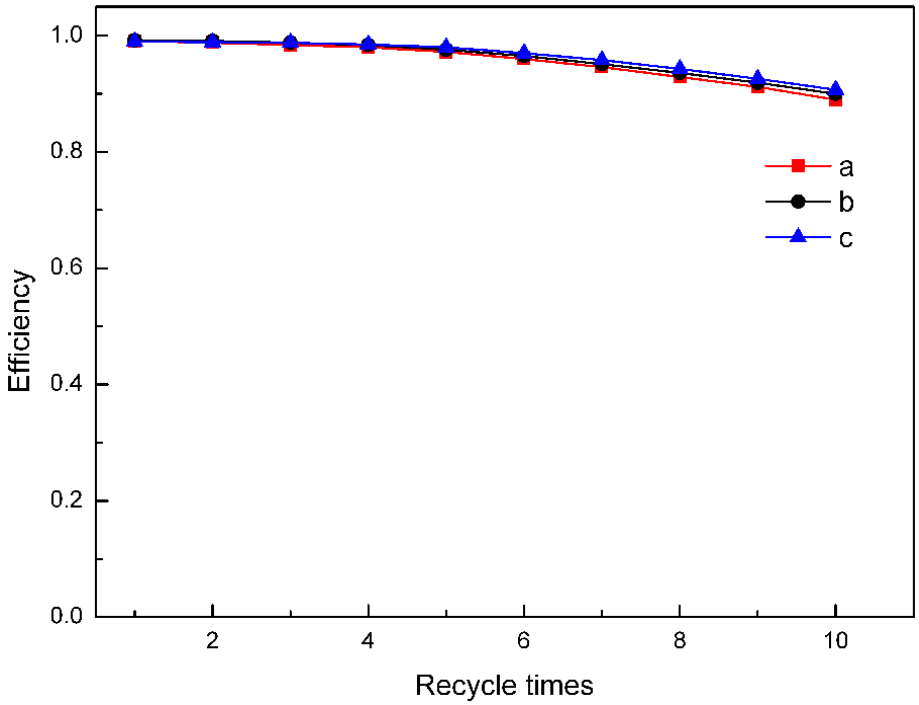

Fig. 11 The photocatalytic efficiency of different AgCl photocatalysts in each 10 recycling degradation experiments: (a) octahedral AgCl NCs, (b) TPH AgCl NCs and (c) concave HOH AgCl NCs.

According to the photocatalytic theories of semiconductor NCs,[31] the possible photocatalytic mechanism of our AgCl NCs for the photodegradation reaction is proposed. Firstly, under visible light illumination, photogenerated electrons and holes can be excited to produce inside AgCl NCs. Meanwhile, metallic Ag NPs with a strong surface plasmon resonance (SPR) effect formed on the AgCl NCs surfaces during the photocatalytic process (shown in Fig. 12) play an important role in increasing visible light absorption and suppressing the recombination of these photo-excited electron–hole pairs.[32] Secondly, the high surface energies and large surface areas from polyhedral AgCl NCs in the nano-photocatalysis may enhance the reactive activity, ie., charge transport and effective contact area, result in dividing the electrons and holes effectively and in favour of high photocatalytic performance. It has been demonstrated that the separated photogenerated holes play a major role in

the photo-oxidation degradation of organic dyes.[33] Therefore, the effective photodegradation of MO dye with the assistance of our AgCl NCs photocatalysts under visible light irradiation can be presented. In particular, for the TPH and concave HOH AgCl NCs, a series of high-index facets with higher surface energies and larger surface areas exposed, higher photocatalytic activity were exhibited relative to octahedral AgCl NCs whose faces mainly exposed {111} with lower surface areas and surface energies.

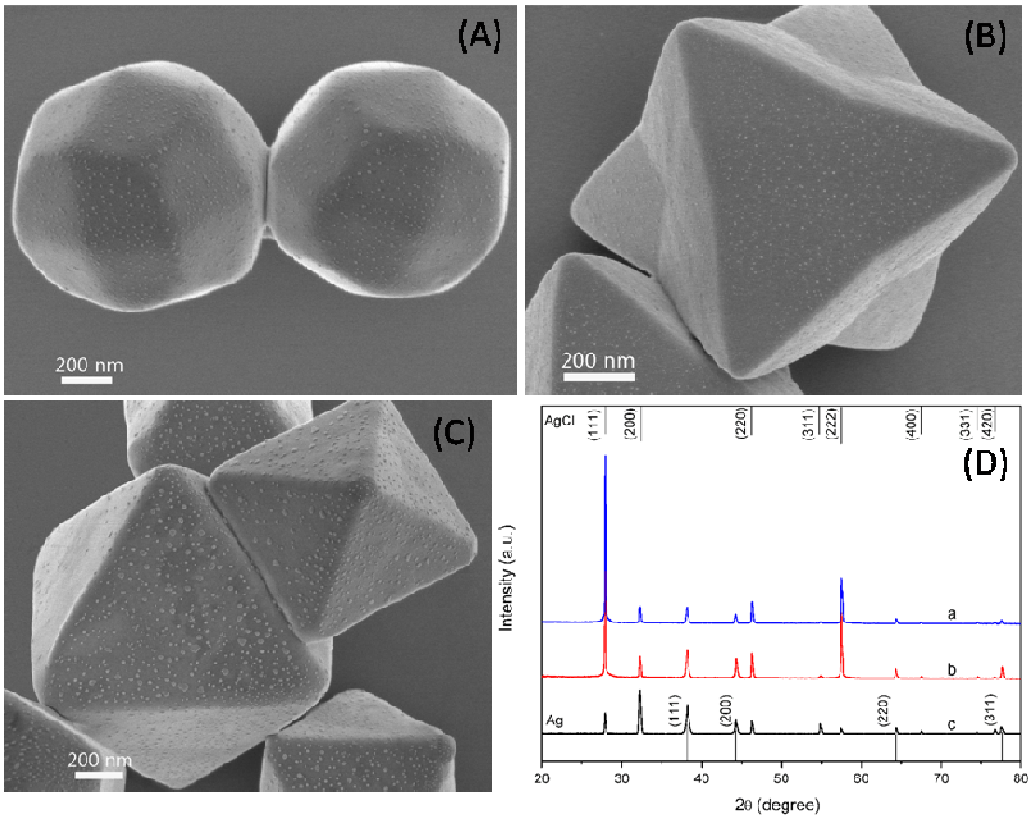

Fig. 12 (A-C) SEM images of different AgCl NCs after photodegradation experiments: (A) TPH AgCl NCs, (B) concave HOH AgCl NCs and (C) octahedral AgCl NCs; (D) XRD patterns of each products after photodegradation experiments: (a) concave HOH AgCl photocatalysis, (b) octahedral AgCl photocatalysis and (c) TPH AgCl photocatalysis.

4. Conclusions

In summary, high-index faceted AgCl semiconductor nanocrystals (NCs) with TPH and concave HOH structures have been successfully prepared for the first time in high yield by a direct one-pot solvothermal method. The as-synthesized TPH, HOH AgCl NCs with unconventional polyhedral shapes and smooth surfaces were enclosed by 24 high-index {311} facets and 48 high-index {15 5 2} facets, respectively. The

formation of high-index facets is attributed to the specific AgCl nucleis crystal growth assisted by ionic liquid surfactant PDDA in an appropriate concentration of hot $AgNO_3$ EG solution. By adjusting the molar ratio of two precursors, the reaction temperatures and times, various derivatives can be obtained, including uniform octahedral, near-spherical AgCl NCs, disordered AgCl or Ag based nanorods and nanoparticles. Owing to the presence of high-index facets with high surface energies and large surface areas exposed, both TPH and concave HOH AgCl NCs photocatalysts exhibit much higher photocatalytic activity than octahedral AgCl NCs whose faces mainly exposed {111} with lower surface surface areas and surface energies in the degradation of organic MO dye under visible light. Particularly, the catalytic activity of concave HOH AgCl is nearly two times higher than that with octahedral morphologies. The photocatalysis efficiency of the as-prepared AgCl NCs photocatalysts are stable in the repetitive degradation experiments. This present study demonstrates that AgCl NCs enclosed by high-index facets is an exciting approach for the design alternative semiconductor photocatalysts with high performance, which may find potential applications such as in photochromics and environmental managements.

Acknowledgements

We gratefully acknowledge the financial support from the Lightweight Optics and Advanced Materials Center (LOMC). Prof. H. Liu and Prof. J. Fang are thanked for their additional insights.

Notes and references

1 M. Gao, Y. Xu, J. Jiang and S. Yu, *Chem. Soc. Rev*., 2013, **42**, 2986.
2 T. P. Yoon, M. A. Ischay an J. Du, *Nat. Chem*., 2010, **2**, 527.
3 C. Liu, U. Burghaus, F. Besenbacher and Z. Wang, *ACS Nano*, 2010, **4**, 5517.
4 B. Liu and E. S. Aydil, *J. Am. Chem. Soc*., 2009, **131**, 3985.
5 Y. Su, Q. Wu an G. Shi, *Energy Environ. Sci*., 2011, **4**, 1113.
6 H. Tong, S. Ouyang, Y. Bi, N. Umezawa, M. Oshikiri and J. Ye, *Adv. Mater*., 2012, **24**, 229.
7 K. Akihiko and M. Yugo, *Chem. Soc. Rev*., 2009, **38**, 253.
8 N. R. Srinivasan, P. A. Shankar and B. Rajdip, *Carbon*, 2013, **57**, 1.
9 Y. Xu, Y. Zhuang and X. Fu, *J. Phys. Chem. C*, 2010, **114**, 2669.
10 J. Pan, Z. Cai, Y. Yu and X. Zhao, *J. Mater. Chem*., 2011, **21**, 11430.
11 M. Liu, X. Qiu, M. Miyauchi and K. Hashimoto, *Chem. Mater*., 2011, **23**, 5282.
12 Z. Seh, S. Liu, M. Low, S. Zhang, Z. Liu, A. Mlayah and M. Han, *Adv. Mater*., 2012, **24**, 2310.
13 P. Wang, B. Huang, X. Qin, X. Zhang, Y. Dai, J. Wei and M. H. Whangbo, *Angew. Chem., Int. Ed*., 2008, **47**, 7931.

14 Z. Lou, B. Huang, P. Wang, Z. Wang, X. Qin, X. Zhang, H. Cheng, Z. Zheng and Y. Dai, *Dalton Trans*., 2011, **40**, 4104.
15 Z. Lou, B. Huang, X. Qin, X. Zhang, H. Cheng, Y. Liu, S. Wang, J. Wang and Y. Dai, *Chem. Commun*., 2012, **48**, 3488.
16 C. An, S. Peng and Y. Sun, *Adv. Mater*., 2010, **22**, 2570.
17 B. Cai, J. Wang, D. Han, S. Gan, Q. Zhang, Z. Wu and L. Niu, *Nanoscale*, 2013, **5**, 10989.
18 Y. Bi, S. Ouyang, J. Cao and J. Ye, *Phys. Chem. Chem. Phys*., 2011, **13**, 10071.
19 G. A. Somorjai and D. W. Blakely, *Nature*, 1975, **258**, 580.
20 N. Tian, Z. Zhou, S. Sun, Y. Ding and Z. Wang, *Science*, 2007, **316**, 732.
21 Z. Quan, Y. Wang and J. Fang, *Acc. Chem. Res*., 2013, **46**, 191.
22 Y. Li, Y. Jiang, M. Chen, H. Liao, R. Huang, Z. Zhou, N. Tian, S. Chen and S. Sun, *Chem. Commun*., 2012, **48**, 9531.
23 Y. Yu, Q. Zhang, B. Liu and J. Y. Lee, *J. Am. Chem. Soc*., 2010, **132**, 18258.
24 N. Tian, J. Xiao, Z. Zhou, H. Liu, Y. Deng, L. Huang, B. Xu and S. Sun, *Faraday Discuss*., 2013, **162**, 77.
25 N. Tian, Z. Zhou and S. Sun, *J. Phys. Chem. C*, 2008, **112**, 19801.
26 H. Zhang, Y. Lu, H. Liu and J. Fang, *RSC Adv*., 2014, **4**, 36757.
27 C. Li, K. L. Shuford, M. Chen, E. J. Lee and S. O. Cho, *ACS Nano*, 2008, **2**, 1760.
28 Y. Xia, Y. Xiong, B. Lim and S. E. Skrabalak, *Angew. Chem., Int. Ed*., 2009, **48**, 60.
29 A. Tao, P. Sinsermsuksakul and P. Yang, *Angew. Chem., Int. Ed*., 2006, **45**, 4597.
30 S. Glaus and G. Calzaferri, *Photochem. Photobiol. Sci*., 2003, **2**, 398.
31 M. R. Hoffmann, S. T. Martin, W. Choi and D. W. Bahnemann, *Chem. Rev*., 1995, **95**, 69.
32 S. K. Cushing, J. Li, F. Meng, T. R. Senty, S. Suri, M. Zhi, M. Li, A. D. Bristow and N. Wu, *J. Am. Chem. Soc*., 2012, **134**, 15033.
33 M. A. Henderson, *Surf. Sci. Rep*., 2011, **66**, 185.